2010

Thermal models of railroad wheels and bearings

Kevin D. Cole
University of Nebraska-Lincoln, kcole1@unl.edu

Constantine M. Tarawneh
University of Texas–Pan American, tarawneh@utpa.edu

Arturo A. Fuentes
University of Texas–Pan American, aafuentes@utpa.edu

B. M. Wilson
Amsted Rail, Granite City, IL

L. Navarro
University of Texas–Pan American

Published in *International Journal of Heat and Mass Transfer* 53:9-10 (April 2010), pp. 1636–1645;
doi: 10.1016/j.ijheatmasstransfer.2010.01.031

Submitted August 9, 2009; revised January 15, 2010; published online February 9, 2010.

Thermal models of railroad wheels and bearings

K. D. Cole,[1] C. M. Tarawneh,[2] A. A. Fuentes,[2] B. M. Wilson,[3] and L. Navarro [2]

1. University of Nebraska–Lincoln, Department of Mechanical Engineering, N104 Walter Scott Engineering Center, Lincoln, NE 68588-0656, USA

2. University of Texas–Pan American, Department of Mechanical Engineering, 1201 West University Drive, Edinburg, TX 78539, USA

3. Amsted Rail, 1700 Walnut Street, Granite City, IL 62040, USA

Corresponding author — K. Cole, tel 402 472-5857, fax 402 472-1465, email kcole1@unl.edu

Abstract
The rolling surface for railroad wheels can be a heat source that may have an impact on the performance of the wheel bearing. In this study, experimental data from an electrically-heated railroad wheel set is analyzed by constructing thermal models of the wheel set. A steady finite-element model, a steady-analytical model, and a transient lumped-parameter model are discussed. Model parameters are determined from careful comparisons with the experimental data. The lumped-parameter model given here is intended as a simple predictive tool for determining when wheel heating caused by rail operations will have an impact on bearing temperature. The model parameters found in this study will also be useful as experimentally-validated boundary conditions in ongoing finite-element studies of heated wheels.

Keywords: annular fin, heat transfer coefficient, parameter estimation, contact conductance

1. Introduction

Catastrophic bearing failure is a major concern for the railroad industry because it can lead to costly train stoppages and even derailments. Excessive heat buildup within the bearing is one of the main factors that can warn of impending failure. Trackside hot-box detectors are used to identify those bearings which are operating at temperatures greater than 105.5 °C (190 °F) above ambient conditions. As a safety precaution, bearings which are determined to be running hot are removed from service for later disassembly and examination. An extension of this practice is the tracking of bearing temperatures over time by collating data from successive hot-box detectors, located tens of miles apart along major rail corridors, and by comparing individual bearing temperatures against the average of all the bearing temperatures on the train [1].

Thermal investigations of roller bearings have been carried out for more than three decades now [2]. The main goals and objectives of many researchers were to identify the various sources of bearing heating, and to study the different effects that may lead to above-normal bearing operating temperatures [3–8]. Over the past three years and in a series of five papers, the authors of this paper have performed detailed laboratory experiments and theoretical studies focused on understanding and quantifying the heat transfer paths within railroad tapered roller bearings in an effort to identify the root cause(s) of warm bearing temperature trending [9–13].

There have been several studies of railroad wheel temperatures. Operating temperatures for the wheel vary, but are normally found to be between 100 °C and 300 °C, depending somewhat on the ambient temperature and atmospheric conditions. In some cases, wheel rim surface temperatures have been determined to reach up to 600 °C [14, 15]. These high temperatures are usually associated with an occasionally-occurring flaw known as a wheel flat. This is a flat region on the normally circular rolling surface of the wheel which is created by the wheel sliding on the railroad tracks. The occurrence of sliding is a consequence of many factors such as poorly adjusted or defective brakes, slopes on the terrain that force the driver to apply the brakes while the car is moving and even contamination on the tracks due to fallen leaves, water or snow [16]. When a wheel flat develops, the surface contact between the two metals creates friction, which over time causes the wheel to heat up to high temperatures. In a study done by Jergeus et al. [16], a total of 140 experiments were performed using a test train that consisted of an electric locomotive, a measuring car containing data sampling equipment, a car equipped for measuring the pulling force, and a test car. New wheels were used and an average of 10 wheel flats were created on each test under controlled conditions, including a brake that was manually controlled from the measuring car, capable of completely locking the test axle. It was determined that temperatures of up to 750 °C were reached by the outside surfaces of the wheel.

Recently analytical modeling and experimental efforts have been combined to determine the heat generated at the wheel and rail interface [17–19]. These studies have resulted in a theoretical model that predicts the thermal behavior of the contact area between the wheel and track when the brakes are applied.

Nomenclature

a minimum radius of wheel web (m)
A_0 contact area between bearing and axle (m^2)
A_1 = $2\pi aw$ (m^2)
A_2 = $2\pi bw$ (m^2)
A_B surface area of bearing for convection (m^2)
A_H surface area of hub for convection (m^2)
A_T surface area of wheel tread for convection (m^2)
b maximum radius of wheel web (m)
c specific heat ($J\ kg^{-1}\ K^{-1}$)
B_i Biot number, $h_i b/k$ (no units)
G Green's function (no units)
h_∞ heat transfer coefficient for loss to air ($Wm^{-2}\ K^{-1}$)
h_0 contact conductance between bearing and hub ($Wm^{-2}\ K^{-1}$)
h_1 contact conductance between web and hub ($Wm^{-2}\ K^{-1}$)
h_2 contact conductance between web and wheel tread ($Wm^{-2}\ K^{-1}$)
k thermal conductivity ($Wm^{-1}\ K^{-1}$)
m fin parameter, Equation (1), (m^{-1})
P heat flow from electric heater (W)
Q heat flow (W) within model
r observation location (m)
r' heating location for GF (m)
T temperature (K)
T_∞ air temperature (K)
V_0 bearing volume (m^3)
V_1 hub volume (m^3)
V_2 wheel tread volume (m^3)
w (average) thickness of wheel web (m)

Greek symbols

a thermal diffusivity ($m^2\ s^{-1}$)
ρ density ($k\ gm^{-3}$)
θ temperature rise, ($T - T_0$) (K)

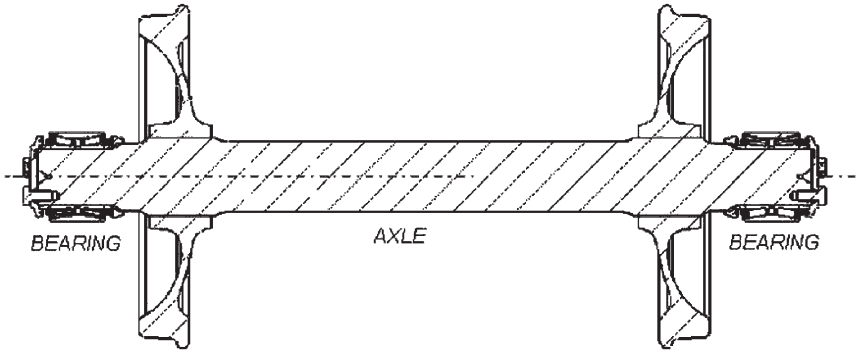

Figure 1. Cross section of wheel set used for transient experiments, with heat introduced on the braking surface (rim) of one wheel.

Yet in all of the efforts reported above, the effects of a hot railroad wheel on the adjacent bearing have not been investigated. Furthermore, current research focuses only on the temperatures reached by the contact area of the wheel and does not give an insight into the heat distribution throughout the wheel radius. With this motivation, the wheel set shown in Figure 1 was instrumented and utilized to perform laboratory tests aimed at exploring and quantifying the heat transfer paths to the bearing when wheel heating occurs. Three different thermal models are also described which have enabled us to better understand the dominant physical mechanisms.

2. Heat transfer experiment

The wheel set assembly shown in Figure 1 was instrumented with 32 K-type thermocouples for temperature measurement. The thermocouples are located on the wheel, axle, and bearing as shown in Figure 2 and Figure 3. Thermocouples 1 through 10, placed 36 degrees apart and situated 2.54 cm (1 in) away from the front rim face of the wheel, monitored the wheel tread temperature; thermocouples 11 through 16 positioned 60 degrees apart monitored the temperature of the bearing cup circumference midway along its width; thermocouples 17 through 28 monitored the temperature distribution throughout the wheel radius; thermocouples 29 and 30 were placed 7 cm (2.75 in) apart and measured the surface temperatures of the wheel hub and axle between the wheel and the bearing, respectively; thermocouple 31 monitored the axle surface temperature 30.5 cm (1 ft.) away from the wheel; and finally, thermocouple 32 measured the ambient temperature approximately 1.5 m (5 ft.) away from the wheel. All of the thermocouples assigned to the wheel were welded to the surface, whereas, the remaining thermocouples were fixed to their locations using hose clamps.

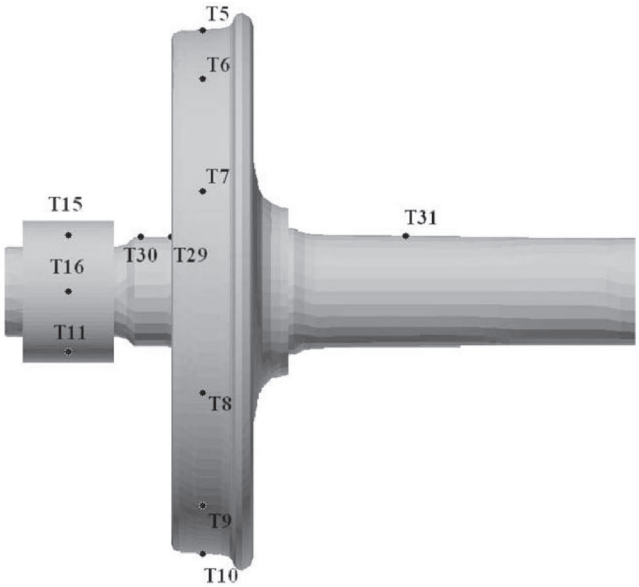

Figure 2. Schematic of the thermocouple locations on the wheel tread, bearing cup, and axle.

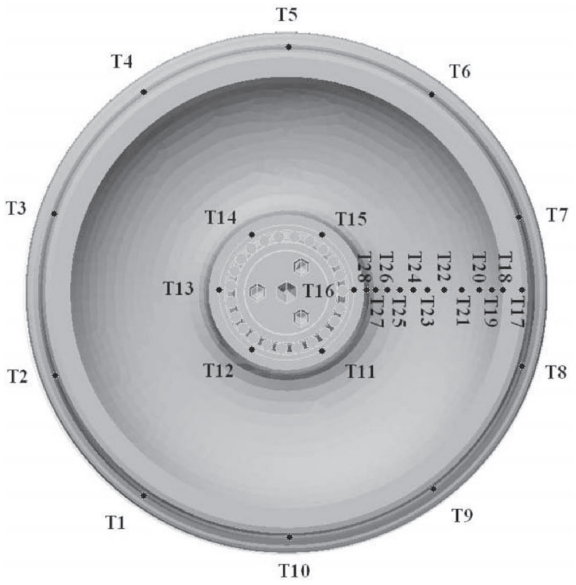

Figure 3. Schematic showing the thermocouple distribution along the wheel radius.

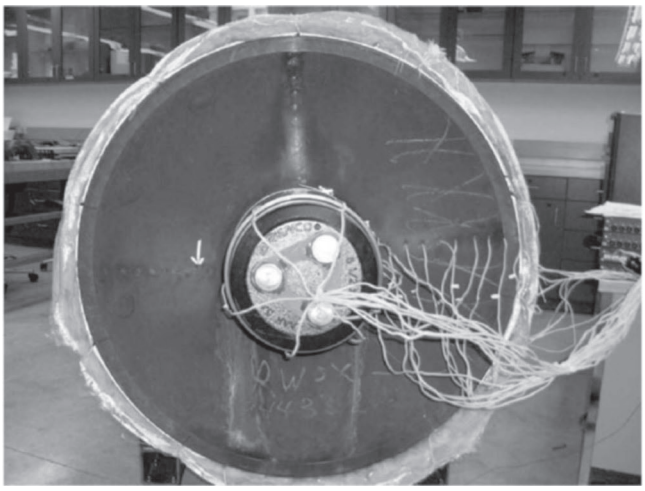

Figure 4. Experimental setup used to perform Tests 2 and 5 in which thermal radiation exchange between the wheel and the bearing was allowed.

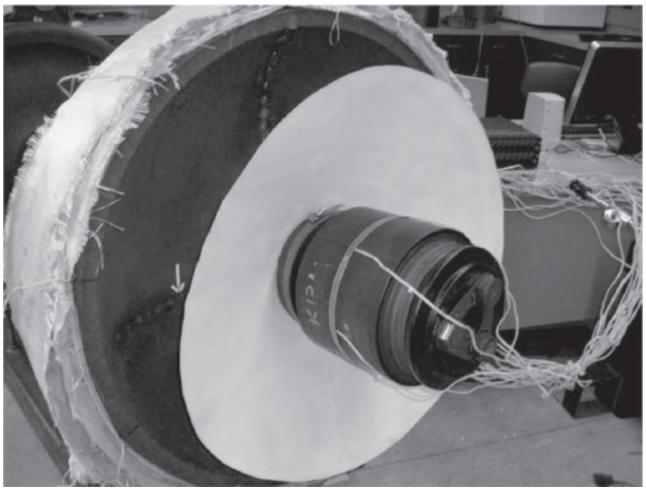

Figure 5. Experimental setup used to perform Tests 3 and 4 in which thermal radiation exchange between the wheel and the bearing was blocked by a cone-shaped radiation shield.

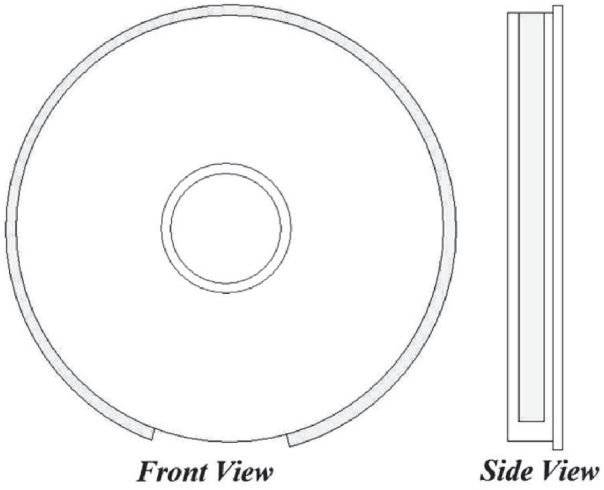

Figure 6. A schematic diagram showing the layout of the electric heating tape around the wheel tread. The uncovered portion at the bottom of the wheel circumference is approximately 43 cm (16.9 in) long.

Two experimental setups were utilized in order to explore the importance of thermal radiation transfer from the wheel to the bearing. A total of five experiments were performed: one shakedown run after which some adjustments were made; two runs with radiation allowed; and, two runs with radiation blocked. Two runs of each type were carried out to demonstrate consistency and repeatability of the experimental technique. The first setup, shown in Figure 4, was used to conduct Tests 2 and 5 in which radiation exchange between the wheel and the bearing was allowed. The second setup, shown in Figure 5, was used for Tests 3 and 4 in which radiation exchange between the wheel and bearing was blocked via a cone-shaped shield fabricated out of 0.4 mm (1/64 in) thick aluminum sheet. The radiation shield was placed on the axle between thermocouples 29 and 30, 8.26 cm (3.25 in) away from the bearing. The diameter of the radiation shield at its largest end is 84 cm (33.1 in) which is big enough to shield the bearing entirely from the wheel. Furthermore, the side of the radiation shield from the bearing was painted white to minimize heat emission to the bearing cup. A full discussion of the experimental geometry and data from the five experiments has been published previously [20]; in the present paper data from two of the five tests are discussed in the contex of thermal modeling.

Wheel heating was achieved through an Omega ultra high-temperature heating tape (SWH351-080), 243.84 cm (96 in) long and 8.26 cm (3.25 in) wide, rated at 2512 W and 120 V. The tape was wrapped around the wheel tread on top of the thermocouples, and held in place using two sets of hose clamps. Unfortunately, the heating tape lengths available were either shorter or longer than the circumference of the wheel. Since overlapping the heating tape creates a fire hazard, the shorter tape was used which meant that about 43 cm (16.9 in) of the bottom of the wheel circumference was not covered by the heating tape, as shown in Figure 6. To ensure that all of the heat input went into heating the wheel and none escaped outward, the heating tape was blanketed with two layers of insulation sandwiched between two layers of fiber glass.

Power was delivered to the electric heating tape, which contains two separate resistance wires, through two variable AC power supplies (Variacs). An isolation transformer was used to filter out the noise from the AC power supplies and eliminate the interference with the data acquisition system.

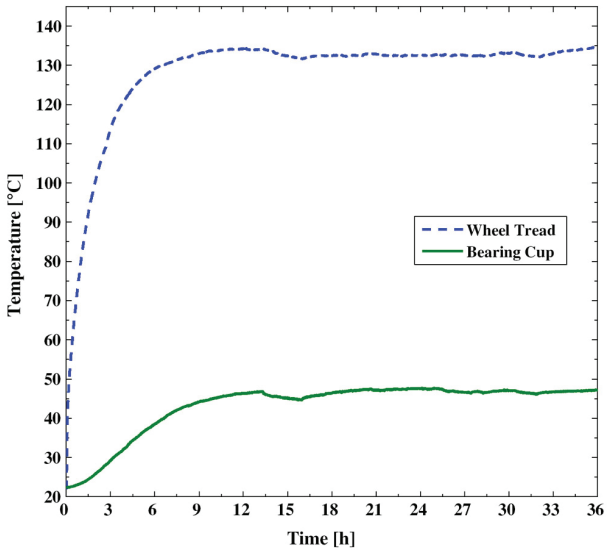

Figure 7. A plot of the transient temperature profiles for the wheel tread and bearing cup for Test 5, in which body-to-body radiation between the wheel and the bearing was allowed (total heat input = 1834 W).

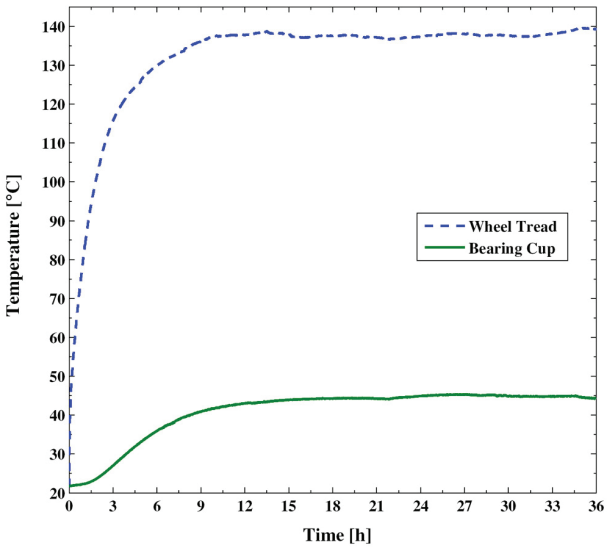

Figure 8. A plot of the transient temperature profiles for the wheel tread and bearing cup for Test 4, in which body-to-body radiation between the wheel and the bearing was blocked via a cone-shaped radiation shield (total heat input = 1815 W).

The peak power that could be delivered to the heating tape through this system was about 1830 W.

To begin an experiment, the data acquisition software was initiated, and 120 s of data were acquired and displayed on-screen to ensure that all thermocouples read room temperature. Both Variacs were then adjusted, with the aid of the digital multi-meters, to produce the maximum possible power output without exceeding their operational limits. Thermocouple data was acquired for 36 h at a sampling rate of 64 Hz (i.e., 64 Samples/s), and the data was averaged every 30 s to produce smoother temperature profiles.

The temperature histories of the wheel tread and bearing cup for Tests 5 and 4 are shown in Figure 7 and Figure 8, respectively. In both Figure 7 and Figure 8, each curve is obtained by averaging the profiles of all the thermocouples assigned to monitor each object's temperature, i.e.; the wheel tread temperature curve is the arithmetic mean of thermocouples 1 through 10, and the bearing cup temperature curve is the mean of thermocouples 11 through 16.

By looking at both Figure 7 and Figure 8, it can be seen that in both tests, the wheel tread reaches steady state conditions much faster than the bearing cup, which is to be expected since the heat input is applied to the wheel tread which then in turn heats up the bearing. Furthermore, the effect of radiation exchange between the hot wheel and the bearing is minimal. The plots show only a 2.2 °C (4 °F) rise in the bearing cup temperature when body-to-body radiation is allowed. Another indicator that conduction heat transfer is dominant is that throughout each transient experiment, the spatial distribution of temperature shows a monotonic decrease from wheel tread to wheel web to axle to bearing as expected along a heat conduction path (see [20]).

3. Finite element model

While the experiments were being carried out, finite-element (FE) modeling was used to analyze the steady temperature in the wheel set. Two simulations focused on replicating the two experimental setups described earlier, where the wheel tread temperature reached approximately 135 °C (275 °F). To this effect, a computer solid model of the wheel-bearing assembly was created. Once the model was completed, it was imported to ALGOR™ 20.3 software and discretized into 5297 elements with a mesh size of 0.02515 m. A combination of bricks, wedges, pyramids and tetrahedral elements were used to successfully mesh the model; surface knitting was used in order to properly apply convection loads.

The materials used for the analysis were taken from the ALGOR™ material library. For the wheel steel, AISI 1080 with a thermal conductivity of 47.7 $Wm^{-1}K^{-1}$ was used; for the axle steel, AISI 1060 with a thermal conductivity of 51.9 $Wm^{-1}K^{-1}$ was chosen; and for the bearing steel, AISI 8620 with a thermal conductivity of 46.6 $Wm^{-1}K^{-1}$ was selected. The surface heat transfer coefficient for convection from the wheel to the air was taken to be 5.3 $Wm^{-2}K^{-1}$ using free-convection correlations (see for example [21]). The heat delivered to the model was distributed uniformly over the wheel area covered by the heating tape, and power delivered was set equal to the measured value from the test run to be simulated.

The FE model was used to simulate the conditions of Tests 4 and 5 which were aimed at quantifying the effect of body-to-body thermal radiation exchange between the wheel and the bearing. The simulation results for Test 5, in which thermal radiation exchange between the wheel and bearing was allowed, are shown in Figure 9. The simulation results for Test 4 were very similar to those shown in Figure 9 since, as explained earlier, the effect of thermal radiation exchange is minimal when the wheel tread temperature is at about 135 °C (275 °F).

Looking at Figure 9, it can be seen that it is an accurate depiction of the experimental test as shown by the fact that the lower portion of the heated wheel is cooler than the rest of the wheel because this represents the area of the wheel tread that was not covered by the heating tape. Furthermore, the other wheel is entirely cold since no heat was applied to its tread and it lies relatively far from the heat source.

By comparing the results of the FE model to those of the experimental testing, the temperature values corresponded very well for all tests conducted, with the percent error being within 6%. A plot comparing the experimental temperature distribution along the radius of the wheel to that produced by the FE model is provided in Figure 10 for Test 5. In Figure 10 the small difference in the temperature of the wheel tread results from applying the average heat input of each test

Figure 9. A graphic of the simulation that was performed utilizing the finite-element model devised to match the results of Test 5, in which body-to-body radiation exchange between the hot wheel and the bearing was allowed. The surface heating applied to the area of the wheel tread covered by the heating tape was set equal to that measured for Test 5, 1834 W.

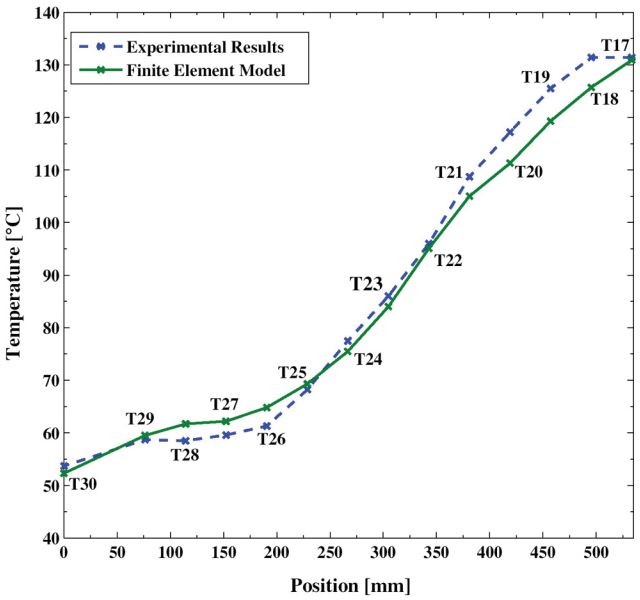

Figure 10. A plot comparing the temperature distribution along the radius of the wheel obtained experimentally from Test 5 to that produced by the FE model.

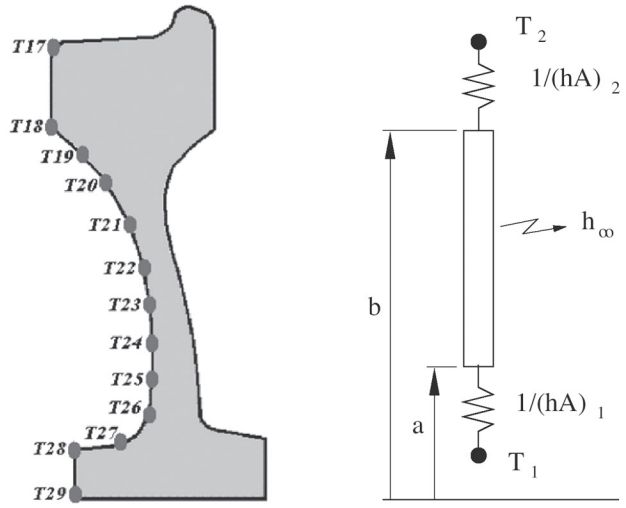

Figure 11. Wheel geometry and steady heat transfer model of wheel web as a uniform annular disk, $a < r < b$, connected to hub and wheel tread by contact conductances h_1 and h_2 and with side losses described by heat transfer coefficient h_∞.

in the FE model. Agreement between Test 4 data and the FE results were comparable, however these results are not shown for the sake of brevity. The very good agreement between the FE model results and the acquired experimental temperature data provides validation for the developed FE model, and indicates that the assumptions made during the development of the model and the correlations used to calculate the free-convection coefficients were appropriate.

4. Steady-analytical model

The steady heat transfer through a railroad wheel is described in this section with an analytical model. The analytical model captures a few features of the heat transfer, and through a systematic comparison with experimental data via regression analysis, the experimental wheel-to-air convection coefficient can be determined. The steady-analytical model is needed because the finite-element model, constructed as it is with a commercial software package, is not readily adapted for regression analysis.

The steady model includes heat transfer by conduction through the web of the wheel and convection heat transfer from exposed surfaces. The web of the wheel is the thin region between the wheel tread (outer radius) and the hub (inner radius). For simplicity, the web is treated as an annular disk of uniform thickness, connected to the wheel tread and hub by contact conductances, and transferring heat to the surroundings by convection. Refer to Figure 11. The steady-analytical geometry, then, is a fin in the shape of a uniform annular disk.

The steady temperature in the uniform annular disk satisfies the following equations:

$$\frac{1}{r}\frac{d}{dr}\left(r\frac{dT}{dr}\right) - m^2(T - T_\infty) = 0; \quad a < r < b \tag{1}$$

$$\text{at } r = a, \quad -k\frac{dT}{dr} = h_1(T_1 - T|_{r=a}) \tag{2}$$

$$\text{at } r = b, \quad -k\frac{dT}{dr} = h_2(T|_{r=b} - T_2) \tag{3}$$

Here $m^2 = 2\,h_\infty/k/w$ where h_∞ is the heat transfer coefficient for convection loss from the sides. The contact conductances provide a simplified description of the heat transfer at the transition between the hub and web (h_1) and the wheel tread and web (h_2). Quantities T_1 and T_2 are the hub temperature and wheel tread temperature, respectively, that communicate with the wheel web through contact conductances h_1 and h_2.

Next, the temperatures will be normalized to put the above equations into a standard form. For θ=$T(r)$-T_∞, θ_1=T_1-T_∞, θ_2=T_2-T_∞, the above temperature equations may be written

$$\frac{1}{r}\frac{d}{dr}\left(r\frac{d\theta}{dr}\right) - m^2\theta = 0; \quad a < r < b \tag{4}$$

$$\text{at } r = a, \quad -k\frac{d\theta}{dr} + h_1\theta|_a = h_1\theta_1 \tag{5}$$

$$\text{at } r = b, \quad -k\frac{d\theta}{dr} - h_2\theta|_b = h_2\theta_2 \tag{6}$$

The above temperature problem is challenging because the general solution takes the form of modified Bessel functions and because of the type 3 non-homogeneous boundary conditions (contact conductance). The method of Green's functions (GF) was used to solve for the temperature, as this method is systematic and readily handles the two non-homogeneous boundaries. The temperature solution has the following form

$$\theta(r) = 2\pi\theta_1 B_1 \frac{a}{b} G(r,r')|_{r'=a} + 2\pi\theta_2 B_2 G(r,r')|_{r'=b} \tag{7}$$

where $G(r,r')$ is the GF. The specific GF for this case is given in Appendix A. For a full discussion of the GF method see [22, chap. 3].

Next, results of the steady-analytical model are presented in comparison with two experiments. For the purposes of comparison with the steady model, thermocouples 17 and 18 were averaged to provide the wheel tread temperature, T_2, thermocouples 27–29 were averaged to provide the hub temperature T_1, and thermocouples 20–25 on the wheel web were compared with the steady thermal model. The geometric values and material properties used and given quantities in the thermal model are given in Table 1. The comparison with experimental data was carried out by coding the steady-analytical model in a general-purpose computer language (Matlab) and performing a non-linear regression analysis to determine the unknown heat transfer quantities B_∞, B_1, and B_2.

The results of the curve fit are given in Table 2, along with some experimental temperatures, for comparison with Tests 4 and 5. The most important value in Table 2 is the Biot number for external heat loss, B_∞, and the close agreement between Tests 4 and 5 suggests that the addition of the radiation shield for Test 5 did not change the external heat loss environment for the wheel. Figure 12 shows a representative comparison between the experimental temperature from Test 4 and the fitted temperature values. The values from Test 5 (not shown for brevity) are also in close agreement. The fact that the steady model provides a close fit to the steady data provides evidence that the simple uniform-thickness description of the wheel web is adequate. This uniform-thickness wheel web has been incorporated into the transient model, discussed in the next section.

Table 1. Geometric and material properties for the steady-analytical model and transient model of the railroad wheel.

a/b	0.52568
b	0.3664 m
A_0	0.03246 m^2
A_B	0.1265 m^2
A_H	0.1977 m^2
A_T	0.6753 m^2
c	480 J kg^{-1} K^{-1}
k	47.7 W m^{-1} K^{-1}
V_2	0.032938 m^3
V_0	0.004680 m^3
w/b	0.09266
a	1.274×10^{-5} m^2 s^{-1}
ρ	7800 kg m^{-3}

Table 2. Biot numbers (B_i=$h_i b/k$) found from fitting between steady model and experimental data; some experimental temperatures are also given.

	Test 4	Test 5	Avg.
B_∞	0.1412	0.1423	0.1418
B_1	10.0312	11.5317	10.7815
B_2	9.0818	9.4882	9.2850
T_∞ (C)	31.13	31.73	31.43
T_1 (C)	59.54	58.95	59.24
T_2 (C)	133.70	131.38	132.54

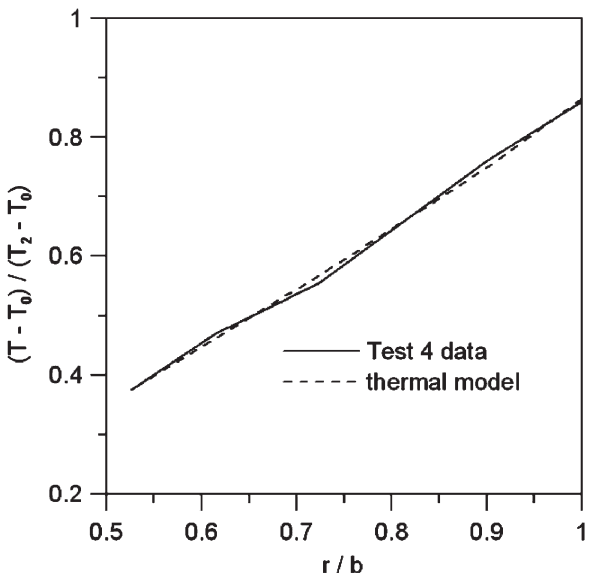

Figure 12. Comparison between experimental temperatures on the wheel web (Test 4) and temperature values computed from the steady model.

5. Transient model

In this section a transient model is developed for the heat transfer in the wheel heated at the outer rim. The transient model contains energy storage in the wheel tread, in the hub/axle, and in the bearing. The energy storage in the wheel web is neglected because of its small mass relative to the mass of the wheel tread. That is, the web temperature is expected to follow the wheel tread temperature in a quasi-steady fashion. Thermal radiation is not included in the transient model, as the experiments show that conduction heat transfer is dominant. With these assumptions, the temperature in the wheel tread, the hub/axle, and bearing satisfy the following equations:

$$\text{wheel tread:} \qquad P - Q_2 - h_\infty A_T\theta_2 = \rho c V_2 \frac{d\theta_2}{dt} \tag{8}$$

$$\text{hub:} \qquad Q_1 - Q_0 - h_\infty A_H\theta_1 = \rho c V_1 \frac{d\theta_1}{dt} \tag{9}$$

$$\text{bearing:} \qquad Q_0 - h_\infty A_B\theta_0 = \rho c V_0 \frac{d\theta_0}{dt} \tag{10}$$

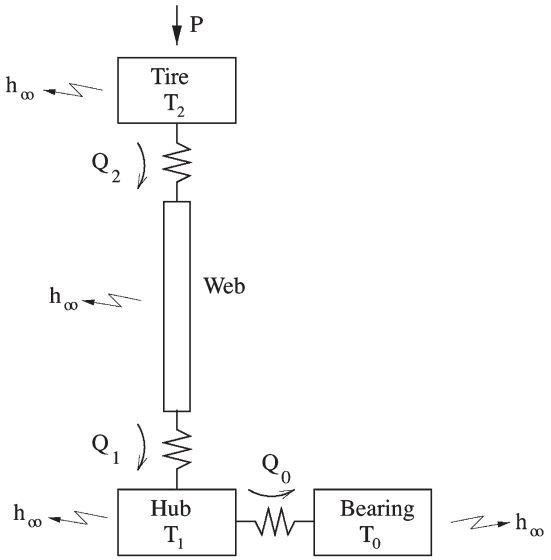

Figure 13. Transient heat transfer model with thermal masses for the wheel tread and hub connected by quasi-steady web. Convection to the surroundings is described by heat transfer coefficient h_∞.

See Figure 13 for a schematic of the transient model. The wheel tread is heated externally at rate P, loses heat to the web at rate Q_2, and loses heat by convection through surface area A_T. The hub/axle gains heat from the web at rate Q_1, loses heat to the bearing at rate Q_0, and loses heat by convection through surface area A_H. The bearing gains heat from the hub/axle at rate Q_0 and loses heat by convection through area A_B. Next quantities Q_0, Q_1 and Q_2 may be stated in terms of contact conductances h_0, h_1 and h_2 according to

$$Q_0 = h_0 A_0 (\theta_1 - \theta_0) \tag{11}$$

$$Q_1 = h_1 A_1 (\theta(a) - \theta_1) \tag{12}$$

$$Q_2 = h_2 A_2 (\theta_2 - \theta(b)) \tag{13}$$

Here web temperatures $\theta(a)$ and $\theta(b)$ are given by Equation (7) evaluated at $r = a$ and $r = b$:

$$\theta(a) = 2\pi\left(B_1 \frac{a}{b} G(a,a)\,\theta_1 + B_2\, G(a,b)\,\theta_2\right) \tag{14}$$

$$\theta(b) = 2\pi\left(B_1 \frac{a}{b} G(b,a)\,\theta_1 + B_2\, G(b,b)\,\theta_2\right) \tag{15}$$

The preceding five equations may be substituted into the first-order differential equations listed above to give three equations for unknown temperatures θ_0, θ_1, and θ_2:

$$P - h_2 A_2\left(\theta_2 - 2\pi\left[B_1 \frac{a}{b} G(b,a)\,\theta_1 + B_2\, G(b,b)\,\theta_2\right]\right) - h_\infty A_T \theta_2 = \rho c V_2 \frac{d\theta_2}{dt} \tag{16}$$

$$h_1 A_1\left(2\pi\left[B_1 \frac{a}{b} G(a,a)\,\theta_1 + B_2\, G(a,b)\,\theta_2\right] - \theta_1\right) - h_0 A_0(\theta_1 - \theta_0) - h_\infty A_H \theta_1 = \rho c V_1 \frac{d\theta_1}{dt} \tag{17}$$

$$h_0 A_0(\theta_1 - \theta_0) - h_\infty A_B \theta_0 = \rho c V_0 \frac{d\theta_0}{dt} \tag{18}$$

Next the equations will be normalized with the following variables:

$$\theta^+ = \frac{(T - T_0)bk}{P}; \quad t^+ = \alpha t \frac{b}{V_2}$$

$$M_1 = V_1/V_2; \quad M_0 = V_0/V_2$$

$$B_i = h_i b/k; \quad C_i = B_i \frac{A_i}{b^2}$$

Using these variables, and dividing by P, the above differential equations may be written

$$1 + \theta_1^+\left[C_2 B_1 \frac{a}{b} 2\pi G(b,a)\right] + \theta_2^+\left[C_2 B_2 2\pi G(b,b) - C_2 - B_\infty \frac{A_T}{b^2}\right] = \frac{d\theta_2^+}{dt^+} \tag{19}$$

$$\theta_0^+ C_0 + \theta_1^+\left[C_1 B_1 \frac{a}{b} 2\pi G(a,a) - C_0 - B_\infty \frac{A_H}{b^2}\right] + \theta_2^+[C_1 B_2 2\pi G(a,b)] = M_1 \frac{d\theta_1^+}{dt^+} \tag{20}$$

$$\theta_0^+\left[-C_0 - B_\infty \frac{A_B}{b^2}\right] + \theta_1^+ C_0 = M_0 \frac{d\theta_0^+}{dt^+} \tag{21}$$

These equations can be stated compactly by consolidating the coefficients of the temperature terms on the left side in the form

$$1 + D_1\theta_1^+ + D_2\theta_2^+ = \frac{d\theta_2^+}{dt^+} \tag{22}$$

$$E_0\theta_0^+ + E_1\theta_1^+ + E_2\theta_2^+ = M_1 \frac{d\theta_1^+}{dt^+} \tag{23}$$

$$F_0\theta_0^+ + F_1\theta_1^+ = M_0 \frac{d\theta_0^+}{dt^+} \tag{24}$$

where

$$D_1 = C_2 B_1 \frac{a}{b} 2\pi G(b,a)$$

$$D_2 = C_2 B_2 2\pi G(b,b) - C_2 - B_\infty \frac{A_T}{b^2}$$

$$E_0 = C_0$$

$$E_1 = C_1 B_1 \frac{a}{b} 2\pi G(a,a) - C_0 - C_1 - B_\infty \frac{A_H}{b^2}$$

$$E_2 = C_1 B_2 2\pi G(b,a)$$

$$F_0 = -C_0 - B_\infty \frac{A_B}{b^2}$$

$$F_1 = C_0$$

The above coupled first-order ordinary differential equations were solved numerically with a Runga-Kutta method. The numerical solution was checked against an analytical solution for the special case h_0=0 (a two-lump version of the model). The numerical and analytical solutions agreed to four significant digits.

If the geometry and the constriction resistances are known, then temperatures θ_0^+, θ_1^+, and θ_2^+ (for the bearing, hub and wheel tread, respectively) may be found as functions of time. Once these temperatures have been found, then the temperature in the wheel web may be found from Equation (7).

6. Transient model results

The transient model was systematically compared with data from Test 4 to determine certain model parameters. The model parameters that were found are mass ratio M_1, and Biot numbers B_0, B_1, B_2, and B_∞. Parameter M_1 represents the effective mass of the hub/axle, that is, the portion of the hub/axle mass that is actively storing heat during the experiment. The Biot numbers B_0,B_1,B_2 are associated with heat flow Q_0, Q_1, Q_2, respectively, in the model (refer to Figure 13). Biot number B_∞ describes the heat loss to the air from all exposed surfaces of the wheel set.

The raw thermocouple values were adjusted before comparison with the model, as follows. First, the size of the data set was reduced by selecting every 20th time record. In this way about 4000 data records at intervals of 30 s were reduced to about 200

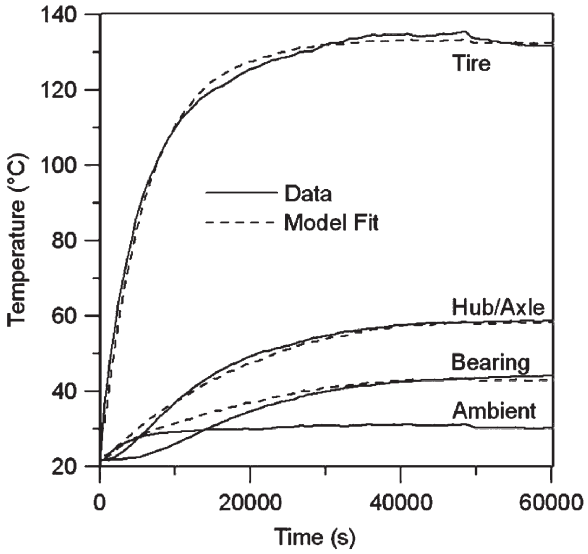

Figure 14. Best fit between Test 4 data and the three-lump model for maximum time 60,000 s. The ambient temperature is also shown. Parameter values for this fit are given in Table 3.

data records at intervals of 600 s. This reduction did not visibly change the plots of the data while greatly reducing the storage space and computation time involved with the data analysis. Second, each measured temperature value was normalized by subtracting the time-varying ambient-air temperature. This adjusted data represents the temperature rise above the ambient, and can be directly compared to the θ_i values in the model.

The comparison between model and data took the form of minimizing the sum-of-squared errors with a subroutine from a widely-available programming environment (Matlab). A typical curve fit of test data is shown in Figure 14 for a subset of the data for time range t = 0 to t = 60,000 s. Data for the wheel tread, hub/axle, and bearing were fit simultaneously for all cases under discussion. The wheel tread values for the model agree very closely with the data over the whole time range. The hub/axle and bearing values closely agree in the second half of the time range. However in the first half of the time range, the model values for the hub/axle and bearing are slightly above the experimental data. This is caused, in part, by the rise in room-air temperature (see Figure 14) during the early part of experiment. This occured because the building air conditioning system could not compensate for the continuous addition of over 1800 W to the room from the heated wheel set, and the room temperature rose to a higher level over several hours.

As the transient model is non-linear in the parameters, starting values of the parameter (guesses) are needed as an input to the fitting routine. A wide range of guessed values was explored, and in every case the results were very close. This suggests that the curve fit is robust, that the minimum sum-of-squares found is a global minimum, and that the best parameter values have been found.

Parameter values for the curve fit shown in Figure 14 are given in Table 3 along with parameter values for several other curve fits carried out on different subsets of the data with different data record durations. The parameter values in Table 3 are very consistent over all the data subsets listed. These multiple curve fits allow for calculation of an average and standard deviation for each parameter value. The greatest variability is with parameter B_0 which has a standard deviation of about 10% of the average value. For all the other parameters the standard deviation is less than 4% of the parameter value, which indicates that the uncertainty in the parameter values is small.

7. Discussion

There are several issues about the model fitting procedure that will be discussed next. The transient curve fits reported here were carried out with small data sets constructed by selecting every 20th data record. Other selections of the data were also studied including every 10th, 5th, and the entire data record. The parameter values found from these larger data sets were in complete agreement with the curve fits reported, within the observed tolerances.

In the steady curve fit, temperature data from different radial locations along the wheel web were included. However for the transient curve fit, data only from the wheel tread, hub/axle, and bearing were included. There was some effort to carry out transient curve fits including transient web temperatures, however these fits tended to match the wheel web temperatures closely while degrading the agreement at the wheel tread and bearing. Since the main thrust of the research has been to link bearing temperatures to wheel tread temperatures, the web temperatures were dropped from the transient fits. Exploring how to include the web temperatures, with an appropriate level of weighting in the curve fits, could be included in future studies.

For the contact-conductance Biot numbers that appear in both the steady-analytical and the transient models, we find that fitted values for B_1 and B_2 are not in close agreement between the two models. The value for B_∞, representing convection loss to the surrounding air, is in closer agreement (within 30%). We suggest that the steady-analytical model, which does not include the bearing, should not be expected to agree with the transient model in all particulars. The discussion of the steady-analytical model was included here as a means to show that the uniform-disk description of the wheel web was a simple and effective way to include the wheel web in the transient model.

Table 3. Parameter fits for different subsets of Test 4 data, for different maximum time values (and different number of data points). The last two lines give the average and standard deviation for each parameter over the nine subsets listed.

Maximum time (s)	# pts	M_1	B_0	B_1	B_2	B_∞
48,000	80	0.24481	0.47814	1.41820	0.21301	0.18614
51,000	85	0.24246	0.49466	1.42327	0.21054	0.18619
54,000	90	0.24193	0.51108	1.42897	0.20945	0.18636
57,000	95	0.24172	0.52660	1.43487	0.2088	0.18660
59,400	99	0.24132	0.53802	1.43908	0.20849	0.18680
72,000	120	0.23113	0.58073	1.45944	0.20183	0.18760
84,000	140	0.23200	0.60260	1.45885	0.20441	0.18769
108,000	180	0.23200	0.60260	1.45885	0.20441	0.18769
120,000	200	0.21452	0.62419	1.46862	0.19778	0.18812
Average	(80–200)	0.23577	0.55096	1.44335	0.20652	0.18702
Std. dev.	(80–200)	0.00957	0.05292	0.01841	0.00479	0.00076

The analytical models presented here do not include radiation heat transfer, because the experiments show it is a minor contribution compared to heat conduction for transmitting heat to the bearing; recall that Tests 4 (radiation blocked) and Test 5 (radiation allowed) show only a 2.2 °C difference in the bearing temperature. For these tests the wheel rim was heated to about 135 °C. Radiation could be important, however, if the wheel rim was heated to higher temperatures. We have recently begun using our FE model with both conduction and radiation heat transfer included to make predictions for wheel rim temperatures at 315 °C. In future work we intend to include radiation heat transfer in the analytical models in order to improve our confidence in the FE predictions as we study these higher heat loads at the wheel rim, which (at present) cannot be created in our laboratory.

8. Summary

During rail operations, the temperature of a wheel tread can rise to high levels by normal events such as braking or by problem events such as wheel flats. The effect of such elevated temperatures on the bearing, which is the part of the assembly that is scanned by the trackside infrared detectors, has not been thoroughly investigated or documented in the literature. With this motivation, carefully planned experiments were conducted with the purpose of exploring and quantifying the effect of heat transfer to the bearing from a railroad wheel heated to 135 °C at the rim. Three thermal models were also presented. A finite-element model produced results that matched steady temperatures observed in the heated wheel within 6%. A steady-analytical model was introduced and used to determine, via non-linear regression, the wheel-to-air convection coefficient in the experiment. A transient lumped-capacitive model was presented that matches the observed wheel temperatures very closely over the whole time range (within 4 %) and reproduces the maximum temperature reached by the bearing. The analytical models presented here are based on conduction heat transfer which the experiments indicate is the dominant mechanism; future work may include adding thermal radiation to the models for prediction of behavior produced by higher wheel temperatures.

Acknowledgments — The authors would like to thank Brenco, the bearing division of Amsted Rail, for funding this project. The technical assistance of Martin Reed of Brenco and Todd Snyder of the Union Pacific Railroad are greatly appreciated.

Appendix A. Green's function for the annular disk

In this appendix the solution for the temperature in the annular disk fin is discussed. This fin geometry was first discussed by Harper and Brown [23] with boundary conditions of type 1 and 2 to describe air-cooling fins on engine cylinders. In the present work both boundaries are of type 3. The GF associated with the temperature problem, Equations (1), (2), and (3), satisfies the following equations

$$\frac{1}{r}\frac{d}{dr}\left(r\frac{dG}{dr}\right) - m^2 G = -\frac{\delta(r-r')}{2\pi r'}; \quad a < r < b \tag{25}$$

$$r = a, \quad -k\frac{dG}{dr} + h_1 G|_a = 0 \tag{26}$$

$$r = b, \quad +k\frac{dG}{dr} + h_2 G|_b = 0 \tag{27}$$

The GF is the response at r to a localized heat source at location r' in the annular disk with homogeneous boundary conditions of the third kind (contact conductance). Note that the GF has homogenous boundary conditions of the third kind, just as in the original temperature problem.

The GF may be found by beginning with the homogeneous solution to Equation (25),

$$G_0 = C_1 K_0(mr) + C_2 I_0(mr) \tag{28}$$

where K_0 and I_0 are modified Bessel functions. The particular solution may be found by variation of parameters (see for example [24, chap. 1]). After considerable algebra, the GF is given by

$$G(r|r') = \frac{1}{2\pi(1 - A_1 A_2)} \times \begin{Bmatrix} [A_2 I_0(mr') + K_0(mr')][I_0(mr) + A_1 K_0(mr)], & r < r' \\ [A_2 I_0(mr) + K_0(mr)][I_0(mr') + A_1 K_0(mr')], & r > r' \end{Bmatrix} \tag{29}$$

where

$$A_1 = \frac{kmI_1(ma) - h_1 I_0(ma)}{kmK_1(ma) + h_1 K_0(ma)}$$

$$A_2 = \frac{kmK_1(mb) - h_2 K_0(mb)}{kmI_1(mb) + h_2 I_0(mb)} \tag{30}$$

This GF may also be deduced from a recent collection of solutions in the cylinder [25] for which parameter m is a complex number. In the present application parameter m is a real number.

Now that the GF is known, the temperature is constructed by superposition of the GF in the annular disk ($a < r < b$) at such locations and with such strength as to reproduce the causative effects in the original temperature problem. In the present instance, the temperature is given by superposition of two terms [22, chap. 3]:

$$\theta(r) = \frac{1}{k} h_1 \theta_1 G(r, a)\, 2\pi a + \frac{1}{k} h_2 \theta_2 G(r, b)\, 2\pi b \tag{31}$$

This relation is used to find the steady temperature at any location in the annular disk.

References

[1] S. Karunakaran and T. W. Snyder, Bearing temperature performance in freight cars, in: *Proceedings Bearing Research Symposium, sponsored by the AAR Research Program in conjunction with the ASME RTD 2007,* Chicago, Illinois, September 11–12, 2007.

[2] N. E. Farnfield, Thermal investigations of roller bearings, *Tribology* **5** (3) (1972), p. 104.

[3] D. L. Dunnuck, Steady-state temperature and stack-up force distributions in a railroad roller bearing assembly, M.S. Thesis, University of Illinois at Urbana-Champaign, Urbana, Illinois, 1992.

[4] S. Wang, C. Cusano, and T. F. Conry, Dynamic model of the torque and heat generation rate in tapered roller bearings under excessive sliding conditions, *Tribol. Trans.* **36** (4) (1993), pp. 513–552.

[5] H. Wang, Axle burn-off and stack-up force analyses of a railroad roller bearing using the finite element method, Ph.D. Dissertation, University of Illinois at Urbana-Champaign, Urbana, Illinois, 1996.

[6] M. R. Hoeprich, Rolling-element bearing internal temperatures, *Tribol. Trans.* **39** (4) (1996), pp. 855–858.

[7] D. B. Kletzli, C. Cusano, and T. F. Conry, Thermally induced failures in railroad tapered roller bearings, *Tribol. Trans.* **424** (1999), pp. 824–832.

[8] X. K. Li, A. R. Davies, and T. N. Phillips, A transient thermal analysis for dynamically loaded bearings, *Comput. Fluids* **29** (2000), pp. 749–790.

[9] C. M. Tarawneh, K. D. Cole, B. M. Wilson, and K. Freisen, A lumped capacitance model for the transient heating of railroad tapered roller bearings, in: *Proceeding of the 2007 ASEE-GSW Annual Conference,* March 28–30, 2007.

[10] C. M. Tarawneh, K. D. Cole, B. M. Wilson, and F. Alnaimat, Experiments and models for the thermal response of railroad tapered roller bearings, *Int. J. Heat Mass Transfer* **51** (2008), pp. 5794–5803.

[11] K. D. Cole, C. M. Tarawneh, and B. M. Wilson, Analysis of flux-base fins for estimation of heat transfer coefficient, *Int. J. Heat Mass Transfer* **52** (2009), pp. 92–99.

[12] C. M. Tarawneh, K. D. Cole, B. M. Wilson, and M. Reed, A metallurgical and experimental investigation into sources of warm bearing trending, in: *Proceedings of the 2008 IEEE/ASME Joint Rail Conference,* Wilmington, Delaware, April 22–24, 2008.

[13] C. M. Tarawneh, B. M. Wilson, K. D. Cole, A. A. Fuentes, and J. M. Cardenas, Dynamic bearing testing aimed at identifying the root cause of warm bearing temperature trending, in: *Proceedings of the 2008 ASME RTD Fall Technical Conference,* RTDF2008-74036, Chicago, Illinois, September 24–26, 2008.

[14] K. Knothe and S. Liebelt, Determination of temperatures for sliding contact with applications for wheel-rail systems, *J. Wear* **189** (1995), pp. 91–99.

[15] J. Ahlstrom and B. Karlsson, Microstructural evaluation and interpretation of the mechanically and thermally affected zone under railway wheel flats, *J. Wear* **232** (1999), pp. 1–14.

[16] J. Jergeus, C. Odenmarck, R. Lunden, P. Sotkovszki, B. Karlsson, and P. Gullers, Full-scale railway wheel flat experiments, *Proc. Inst. Mech. Engr.* **213** (Part F) (1999).

[17] T. Vernersson, Temperatures at railway tread braking. Part 1: Modeling, in: *Proceedings of the Institution of Mechanical Engineers, Part F, J. Rail and Rapid Transit,* Jun 2007, vol. 221, no. 2, pp. 167–182, 2007.

[18] T. Vernersson, Temperatures at railway tread braking. Part 2: Calibration and numerical examples, in: *Proceedings of the Institution of Mechanical Engineers, Part F, J. Rail and Rapid Transit,* vol. 221, no. 4, pp. 429–442, 2007.

[19] T. Vernersson, Temperatures at railway tread braking. Part 3: Wheel and block temperatures and the influence of rail chill, in: *Proceedings of the Institution of Mechanical Engineers Part F, J. Rail and Rapid Transit,* vol. 221, no. 4, pp. 443–454, 2007.

[20] C. M. Tarawneh, A. A. Fuentes, B. M. Wilson, K. D. Cole, L. Navarro, Thermal analysis of railroad bearings: Effect of wheel heating, in: *Proceedings of the 2009 IEEE/ASME Joint Rail Conference,* Pueblo, CO, March 3–5, 2009.

[21] W. M. Rohsenow and J. P. Hartnett, *Handbook of Heat Transfer,* McGraw Hill, New York (1973) (Chapter 6).

[22] J. V. Beck, K. D. Cole, A. Haji-Sheikh, and B. Litkouhi, *Heat Conduction Using Green's Functions,* Hemisphere, New York (1992).

[23] D. R. Harper and W. D. Brown, Mathematical equations for heat conduction in the fins of air-cooled engines, *Nat. Advis. Comm. Aeronaut., Tech. Note* **158** (1922), p. 677.

[24] Y. A. Melnikov, *Influence Functions and Matrices,* Prentice Hall (1999).

[25] K. D. Cole and P. E. Crittenden, Steady periodic heating of a cylinder, *J. Heat Transfer* **131** (9) (2009).